The 2010 IEEE/RSJ International Conference on
Intelligent Robots and Systems
October 18-22, 2010, Taipei, Taiwan

Motion Control with Slow and Rapid Adaptation for Smooth Reaching Movement under External Force Disturbance

Fumi Seto and Tomomichi Sugihara

Abstract— **We proposed a nonlinear reference shaping controller for a manipulator which shares its workspace with humans. In this paper, two adaptation methods to external force; "slow adaptation" and "rapid adaptation" are proposed for smoother reaching movements and submissive behavior to follow the force. These make smooth endpoint speed profiles and movements flexible to follow external force without detecting the force. The slow adaptation moderates the manipulator's endpoint acceleration, and it also enables the manipulator to handle subsequent changes of target endpoint positions. If the endpoint position is significantly changed by excessive external force, the rapid adaptation works to follow the force and restart the reaching movement smoothly. The validity of the proposed method is confirmed through computer simulations.**

I. Introduction

On the control of manipulators which share their workspace with humans, we should consider uncertainties such as unexpected external force applied from the environment, cooperation with a human or humans, and others. From a safety viewpoint, it is desirable that the manipulator follows applied external force compliantly not to harm both humans and robots. It is called "flexibility" of the movement in this paper. Realizing such flexible movements, the movements should be generated based on feedback control without explicit inclusion of time, unlike conventional reference trajectory generation approach.

Arimoto et al.[1] proposed a redundant manipulator control method based on the *virtual spring-damper hypothesis*, in which a control signal operates as a parallel pair of mechanical damper and spring drawing its endpoint to the target position. This control law generates reaching movements without trajectory planning, and solves the ill-posedness of inverse kinematics by introducing joint damping factors. With this method, however, the endpoint acceleration is theoretically maximized at the start of the movement. In considering the operations near humans, it is highly preferable to realize human-like smooth reaching movements with bell-shaped endpoint speed profiles[2], [3] to avoid scaring the humans around the manipulator.

Many researchers formulated mathematical models of the human's reaching movements, including the minimum hand jerk model[4] and the minimum joint torque-change model[5]. Generating bell-shaped endpoint speed profiles on the virtual spring-damper hypothesis, Sekimoto et al.[6] proposed the *time-variable stiffness*, in which spring stiffness is changed by using the gamma distribution as a function of time. These methods explicitly include time-dependent terms, and it is difficult to archive flexible movements in the existence of external force.

Based on the virtual spring-damper hypothesis, we proposed a nonlinear reference shaping controller to generate smooth reaching movements[7], [8]. Without trajectory planning and explicit inclusion of time, an intermediate reference position is generated and inputted to the virtual spring-damper system to moderate initial acceleration of the manipulator's endpoint. It also makes the movements flexible along applied external force, and the manipulator generates accurate reaching movements without large acceleration once the force is removed. We also proposed an online parameter tuning approach for generating smooth movements with bell-shaped endpoint speed profiles[9].

Depending on the situations when external force is applied, however, the manipulator cannot follow the force sufficiently. If the endpoint position is changed significantly due to excessive external force, large acceleration might be generated or the manipulator cannot continue the reaching movement.

In this paper, we propose two adaptation methods to external force; "slow adaptation" and "rapid adaptation" to overcome these problems. With these adaptations, apparent initial endpoint position, which is used for the online parameter tuning, is shaped. The slow adaptation moderates the endpoint acceleration, and it also enables the manipulator to handle perturbations of target endpoint position. If the endpoint position is significantly changed by excessive external force, the rapid adaptation works to follow the force and restart the reaching movement smoothly.

Kikuuwe et al.[10], [11] extended PID control approach to *proxy-based sliding mode control* (PSMC), a modified sliding mode control to realize accurate position control during normal operation and recovering from large positional error without overshoot and vibration. In PSMC, however, state space must be divided, making the controller design increasingly complex and potentially triggering frame problems. The proposed method can realize flexible movements along external force without dividing the state space.

Tsuji et al.[12] proposed a trajectory generation method based on an artificial potential field approach combining a time scale transformation and a *time base generator* (TBG). They also applied it to the unicycle-like vehicle and computer simulations were done to show its robustness for temporal ex-

This work was supported in part by Grant-in-Aid for Young Scientists (A) #22680018, Japan Society for the Promotion of Science.

F. Seto is with Future Robotics Technology Center, Chiba Institute of Technology, 2-17-1 Tsudanuma, Narashino, Chiba, Japan fumi@furo.org

T. Sugihara is with Department of Adaptive Machine Systems, Graduate school of Engineering, Osaka University, 2-1 Yamadaoka, Suita, Osaka, Japan zhidao@ieee.org

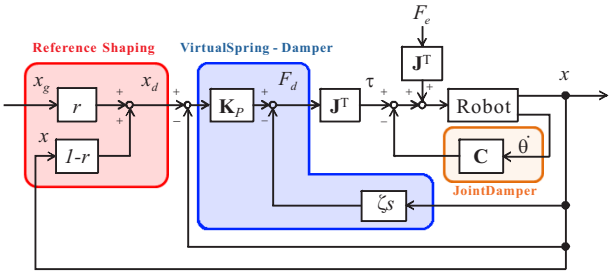

Fig. 1. The schematic block diagram of the proposed controller

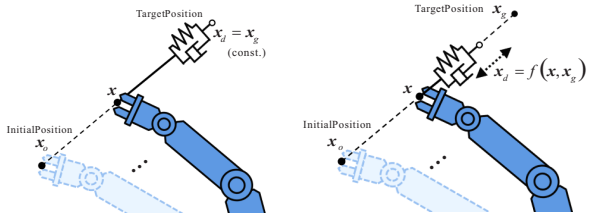

(*a*) Virtual Spring-Damper (*b*) Online Reference Shaping

Fig. 2. The reference position $\boldsymbol{x}_d$ on the virtual spring-damper & online reference shaping

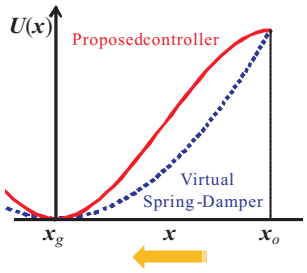

Fig. 3. The shapes of potential fields created by the proposed controller & the traditional virtual spring-damper system

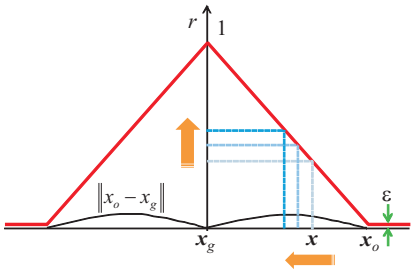

Fig. 4. The change of parameter r in the proposed controller

ternal disturbance[13]. A trajectory generating system based on feedback control and the minimum jerk criterion was presented by Hoff and Arbib[14], which can manage target position perturbations. Although these methods can generate human-like trajectories and bell-shaped speed profiles, the time-dependent term, the target arrival time, is needed so that it cannot handle a long-term external disturbance which the proposed method can deal with.

This paper is organized as follows: the reference shaping controller with online parameter tuning is described in Section II, and Section III presents the proposed adaptations; "slow adaptation" and "rapid adaptation". Section IV reviews computer simulation results confirming the validity of the proposed method, and Section V summarizes conclusions.

II. Nonlinear Reference Shaping with Online Parameter Tuning Approach[9].

Consider an m-joint manipulator and its l-dimensional task space. Applying the virtual spring-damper hypothesis, the force, $\boldsymbol{F}_d \in \mathbb{R}^l$, generated at the manipulator's endpoint and the torque, $\boldsymbol{\tau} \in \mathbb{R}^m$, applied at the joint, are calculated by

$$\boldsymbol{F}_d = \boldsymbol{K}_p (\boldsymbol{x}_d - \boldsymbol{x}) - \boldsymbol{\xi}\dot{\boldsymbol{x}}, \tag{1}$$

$$\tau = -\boldsymbol{C}\dot{\boldsymbol{\theta}} + \boldsymbol{J}^{\mathrm{T}}(\boldsymbol{\theta})\boldsymbol{F}_d, \tag{2}$$

where $\boldsymbol{x}_d \in \mathbb{R}^l$ is the reference position inputted to the virtual spring-damper system, $\boldsymbol{x}, \dot{\boldsymbol{x}} \in \mathbb{R}^l$ the position and velocity vectors of the manipulator's endpoint, and $\boldsymbol{\theta}$, $\dot{\boldsymbol{\theta}} \in \mathbb{R}^m$ the joint angle and angular velocity vectors. $\boldsymbol{K}_p \in \mathbb{R}^{l\times l}$, $\boldsymbol{\xi} \in \mathbb{R}^{l\times l}$, and $\boldsymbol{C} \in \mathbb{R}^{m\times m}$ are the stiffness coefficient matrix, the damping coefficient matrix of the virtual spring-damper, and the joint damping coefficient matrix, respectively. $\boldsymbol{J}(\boldsymbol{\theta}) \in \mathbb{R}^{l\times m}$ denotes the Jacobian matrix for $\boldsymbol{x}$.

Note that while the equilibrium point, given by $\boldsymbol{x}_d$, is asymptotically stabilized in the virtual spring-damper system proposed by Arimoto et al., endpoint acceleration is maximized at the start of each reaching movement. As shown in the potential function of the virtual spring-damper system drawn in dashed line in Fig. 3, the magnitude of the gradient is maximized when $\boldsymbol{x} = \boldsymbol{x}_o$, the initial endpoint position, so that the initial acceleration is also maximized.

In this study, a pre-shaping controller of the reference input, $\boldsymbol{x}_d$, is applied to moderate the initial acceleration. It is shaped as a function of $\boldsymbol{x}$, the current endpoint position,

$$\boldsymbol{x}_d = \left\{ r\boldsymbol{x}_g + (1-r)\boldsymbol{x} \right\}, \quad 0 < r \leq 1, \tag{3}$$

where $\boldsymbol{x}_g$ denotes the final target endpoint position. The schematic block diagram is shown in Fig. 1. In Eq.(3), r is a parameter and the proposed system coincides with the traditional virtual spring-damper system when r is set to 1.

The value of r is expressed as a function of $\boldsymbol{x}$:

$$r = 1 - (1-\epsilon)\frac{\|\boldsymbol{x}_g - \boldsymbol{x}\|}{\|\boldsymbol{x}_g - \boldsymbol{x}_o\|}, \tag{4}$$

where ϵ is a constant satisfying $0 < \epsilon \ll 1$.

As shown in Fig. 4, when the manipulator begins to move ($\boldsymbol{x} = \boldsymbol{x}_o$), r equals ϵ, and $\boldsymbol{x}_d$ is given as a vector value, pointing slightly shifted from the initial endpoint position toward the target position, so that the manipulator starts to move with the moderated acceleration. It is also shown from the potential function in Fig. 3, in which the magnitude of the gradient is almost zero when $\boldsymbol{x} = \boldsymbol{x}_o$. As the endpoint comes close to the target position, r is increased to improve the convergence rate, and then, it takes the maximum value when $\boldsymbol{x}$ is equal to $\boldsymbol{x}_g$, i.e. when the endpoint arrives at the target position. $\boldsymbol{x}$ converges asymptotically to $\boldsymbol{x}_g$ in the proposed controller, it is proved mathematically in Appendix.

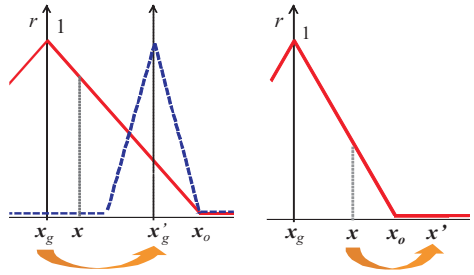

Fig. 5. The change of parameter r without the adaptations

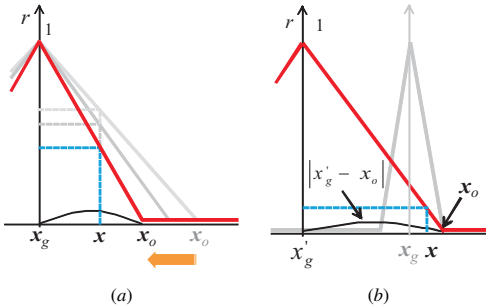

Fig. 6. The effects of the slow adaptation on the change of r

III. Adaptation to External Force

In this section, two adaptation methods to external force; "slow adaptation" and "rapid adaptation" are proposed to shape $\boldsymbol{x}_o$, the apparent initial endpoint position used in Eq.(4). As shown in Fig. 4, r is increased linearly from ϵ to 1 to generate smooth movements with bell-shaped endpoint speed profiles in our previous study[9]. Shaping $\boldsymbol{x}_o$ causes the value of r to be changed by Eq.(4), and it is essential to realize the flexible movements proposed in this paper.

When the target endpoint position is changed from $\boldsymbol{x}_g$ to $\boldsymbol{x}_g'$ as shown in Fig. 5 (a) or $\boldsymbol{x}$ is moved to $\boldsymbol{x}'$ by applied external force as shown in Fig. 5 (b), the smooth reaching movements cannot be re-generated because r becomes equal to ϵ and it is not increased linearly from the current endpoint position to the (new) target position. During external force is applied, on the other hand, the value of r would be better to keep ϵ to decrease $\boldsymbol{F}_d$ that makes it easier for the movement of the manipulator to follow the external force.

In these cases, $\boldsymbol{x}_o$ is shaped for changing the value of r appropriately because of the adaptations described in this section, so that the manipulator can generate compliant behavior along applied external force and restart the reaching movement smoothly after the force is removed.

A. Slow Adaptation

The slow adaptation is defined as shaping $\boldsymbol{x}_o$ according to the first-order lag filter below:

$$\boldsymbol{x}_o = \frac{1}{Ts+1}\boldsymbol{x}. \tag{5}$$

T is a positive constant and the Laplace transform expression applied component-wise is used in Eq.(5).

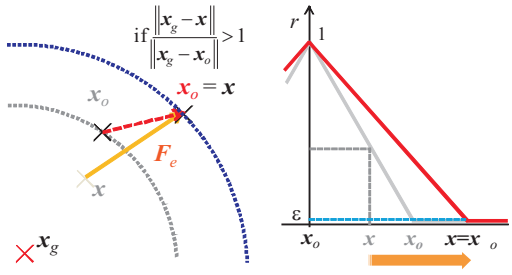

Fig. 7. The rapid adaptation: its concept and the effect on the change of r

As shown in Fig. 6 (a), $\boldsymbol{x}_o$ moves toward $\boldsymbol{x}$ gradually with the first-order lag filter by Eq.(5). It moderates the change of r, so that the manipulator generates smooth endpoint speed profiles. It can also handle the changes of target endpoint positions. Thanks to the slow adaptation, r becomes small and it is increased linearly because $\boldsymbol{x}_o$ places near $\boldsymbol{x}$ when the target position is changed from $\boldsymbol{x}_g$ to $\boldsymbol{x}_g'$ as shown in Fig. 6 (b). Then the manipulator can generate a reaching movement toward the new target position with smooth endpoint speed profile. With conventional trajectory planning approach, on the other hand, we have to re-generate a reference trajectory once the target position is changed.

B. Rapid Adaptation

The rapid adaptation is defined that $\boldsymbol{x}_o$ is reset to $\boldsymbol{x}$ when $\boldsymbol{x}_o$ satisfies the following condition:

$$\boldsymbol{x}_o = \boldsymbol{x} \quad \text{if} \quad \frac{\|\boldsymbol{x}_g - \boldsymbol{x}\|}{\|\boldsymbol{x}_g - \boldsymbol{x}_o\|} > 1. \tag{6}$$

As shown in Fig. 7 (a), the circle, centered at $\boldsymbol{x}_g$ with the radius $\|\boldsymbol{x}_o - \boldsymbol{x}_g\|$ is enlarged to include $\boldsymbol{x}$ when $\boldsymbol{x}$ moves toward to the circle. In this case, $\boldsymbol{x}_o$ is reset to $\boldsymbol{x}$ and it results that r becomes equal to ϵ as shown in Fig. 7 (b). $\boldsymbol{F}_d$ is decreased with $r = \epsilon$, enabling compliant behavior following external force. After the removal of the force, as we can see in Fig. 7 (b), r is linearly increased according to Eq.(4), so that smooth reaching movement is resumed in spite of the change of the endpoint position.

By these two adaptations, the manipulator realizes smooth endpoint speed profiles and flexible movements along applied external force without detecting the force, just only using $\boldsymbol{x}$, $\boldsymbol{x}_g$ and $\boldsymbol{x}_o$. With a back-drivable manipulator, external sensors such as force/torque sensors are not needed when implementing the proposed method[1].

IV. Simulations

The proposed reference shaping controller with the adaptations is implemented in the planar 4 DOF manipulator illustrated in Fig. 8, and computer simulations are performed to investigate that bell-shaped smooth endpoint speed profile is realized while handling subsequent changes of target

[1]When the manipulator is non back-drivable, flexible movements can be generate by attaching a force/torque sensor on its endpoint and inputting the measured force/torque as F_e in Fig. 1.

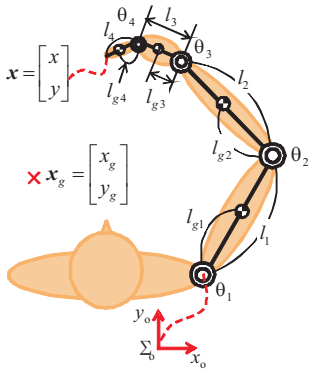

Fig. 8. The simulation setup

TABLE I

THE PARAMETER LIST OF 4-DOF MANIPULATOR

	Link 1	Link 2	Link 3	Link 4
Link Length l $[m]$	0.280	0.280	0.095	0.090
Position of CoM l_g $[m]$	0.140	0.140	0.0475	0.045
Link Mass m $[kg]$	1.4070	1.0780	0.2423	0.2552
Moment of Inertia I $[kgm^2]$	9.758×10^{-3}	7.370×10^{-3}	2.004×10^{-4}	1.780×10^{-5}

endpoint positions. It is also investigated that the manipulator generates flexible movements to follow external force and restarts the reaching movement smoothly from the position in which the force is removed. We also simulated applying the reference shaping controller only (without the adaptations), the virtual spring-damper hypothesis (VSD) and the time-variant stiffness (TVS) for purpose of comparison.

Table I summarizes physical parameters of the manipulator, which are selected based on anthropometry of human. To tune the parameter r, $\epsilon = 0.001$ is used in Eq.(4). The time constant, T, is set to 0.33 for the slow adaptation experimentally, and $\boldsymbol{C} = diag\{0.378, 0.242, 0.058, 0.014\}$ are used for VSD (cf. [1]). To align convergence rate of the reaching movements among all simulations, $\boldsymbol{K}_p = diag\{45.0, 45.0\}$ is used for the proposed controller with the adaptations, $\boldsymbol{K}_p = diag\{30.0, 30.0\}$ for without the adaptations and $\boldsymbol{K}_p = diag\{10.0, 10.0\}$ for VSD. Instead of $\boldsymbol{K}_p$, the following $\boldsymbol{K}_p^{'}(t)$ is used for TVS:

$$\boldsymbol{K}_p^{'}(t) = \boldsymbol{K}_p \left\{ 1 - \left(1 + \alpha t + \frac{\alpha^2}{2} t^2 \right) e^{-\alpha t} \right\} \tag{7}$$

Sampling time is 1.0 $[ms]$ and constant parameter α is 8.0. All simulations used $\boldsymbol{\theta}_o = [70.0\ 50.0\ 30.0\ 80.0]^{\mathrm{T}}$ $[deg]$ as the initial joint angle.

Results of simulations investigating the effect of subsequential target position changes are shown in Fig. 9. We set $\boldsymbol{x}_{g_1} = [-0.35\ 0.35]^{\mathrm{T}}$, $\boldsymbol{x}_{g_2} = [-0.35\ 0.484]^{\mathrm{T}}$, $\boldsymbol{x}_{g_3} = [-0.184\ 0.35]^{\mathrm{T}}$, $\boldsymbol{x}_{g_4} = [-0.184\ 0.484]^{\mathrm{T}}$(m), and target endpoint position of the manipulator $\boldsymbol{x}_g$ is changed to $\boldsymbol{x}_{g_{n+1}}$ when current endpoint position is reached to $\boldsymbol{x}_{g_n}$ $(n = 1 \cdots 3)$.

Fig. 9 (a) shows the endpoint paths, Fig. 9 (b) shows the tangential endpoint speed profiles using the proposed controller with/without the adaptations, and Fig. 9 (c) shows the tangential endpoint speed profiles with VSD/TVS. The endpoint can reach to $\boldsymbol{x}_{g_1}$ and $\boldsymbol{x}_{g_2}$, and its paths are roughly straight similar to hand paths in human reaching movements in all cases. Without the adaptations, the endpoint, however, cannot reach to $\boldsymbol{x}_{g_3}$ and the manipulator is stopped. In this case, large acceleration is generated when the endpoint is moved to $\boldsymbol{x}_{g_2}$ as plotted in Fig. 9 (b). Furthermore, the endpoint speed becomes almost zero after reaching to $\boldsymbol{x}_{g_2}$. This is because that $\boldsymbol{x}_o$ is fixed to original initial endpoint position so that r is no longer increased linearly toward the new target endpoint position, the same as in Fig. 5 (a). With VSD and TVS, although continuous reaching movement is realized but the acceleration is large as plotted in Fig. 9 (c). With the adaptations, on the other hand, the manipulator generates continuous reaching movements to each target endpoint position and its speed profiles are smooth as plotted in Fig. 9 (b), thanks to the slow adaptation.

To evaluate the movement flexibility along applied external force, we conducted simulations in which $\boldsymbol{x}_g = [-0.35\ 0.35]^{\mathrm{T}}$(m) and external force $\boldsymbol{F}_e$ is applied to the endpoint for 1.0 $[s]$. Fig. 10 shows the results of the case of $\boldsymbol{F}_e = [1.0\ 1.0]^T$ (N), Fig. 11 shows the results of the case of $\boldsymbol{F}_e = [1.0\ -1.0]^T$ (N) and Fig. 12 shows the results of the case of $\boldsymbol{F}_e = [-1.0\ -1.0]^T$ (N). In Figs. 10, 11 and 12, the endpoint paths are plotted in (a), the endpoint speed profile with/without the adaptations is plotted in (b) and (c), respectively. $\boldsymbol{F}_e$ is applied when the endpoint reaches the point indicated by the dotted line in (a).

The manipulator continues reaching movement against applied force with VSD and TVS in the case of $\boldsymbol{F}_e = [1.0\ 1.0]^T$ (N). In contrast, it generates flexible movement following the force with the reference shaping controller, and the flexibility is enhanced with the adaptations. With the adaptations, it can restart the movement after the force is removed as shown in Fig. 10 (b), while it takes a long time to resume the movement without the adaptations as shown in Fig. 10 (c). It is because that $\boldsymbol{x}_o$ is never reset without the rapid adaptation and r does not increase from ϵ as shown in Fig. 5 (b). Thanks to the rapid adaptation, $\boldsymbol{x}_o$ is reset to changed $\boldsymbol{x}$, so that r increases linearly as shown in Fig. 7 (b) when the force is removed.

In the case of $\boldsymbol{F}_e = [1.0\ -1.0]^T$ (N), the manipulator generates flexible movement against the force with all methods as shown in Fig. 11 (a), however, the most flexible movement is generated with the adaptations. From Fig. 11 (b), Although the speed is not continuous after the removal of the force even with the adaptations, it is shown that the acceleration is generated to make the speed zero so that the manipulator is never moved rapidly. Without the adaptations, the speed is suddenly increased as shown in Fig. 11 (c), it will be dangerous for humans around the manipulator. This behavior is similar in the case of $\boldsymbol{F}_e = [-1.0\ -1.0]^T$ (N) as shown in Fig. 12.

From these results, it is verified that smooth endpoint speed profile is obtained under the significant and subsequent changes of target endpoint positions with the slow adaptation. It is also investigated that the manipulator generates flexible movements following applied external force and resumes reaching movements from the position in which the external force is removed with the rapid adaptation.

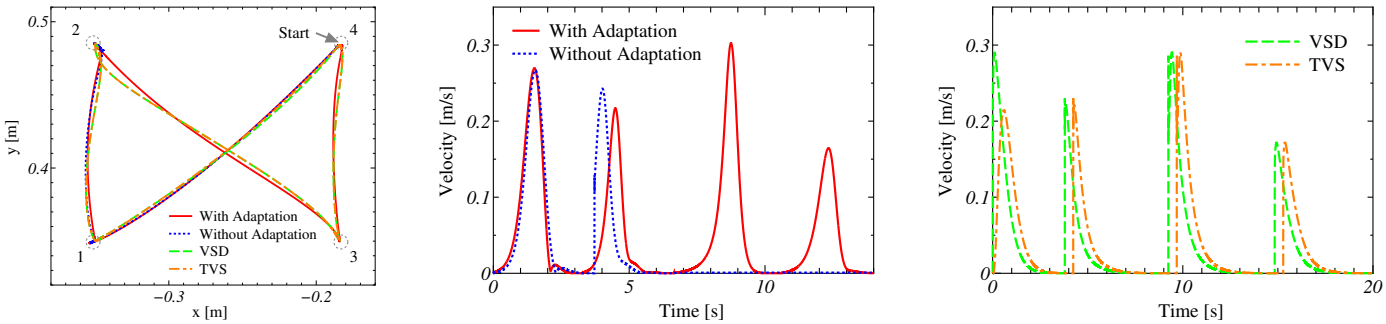

(*a*) Endpoint paths (*b*) Endpoint speed profiles with/without the adaptations (*c*) Endpoint speed profiles with VSD & TVS

Fig. 9. Simulation results: under the subsequent changes of target endpoint positions

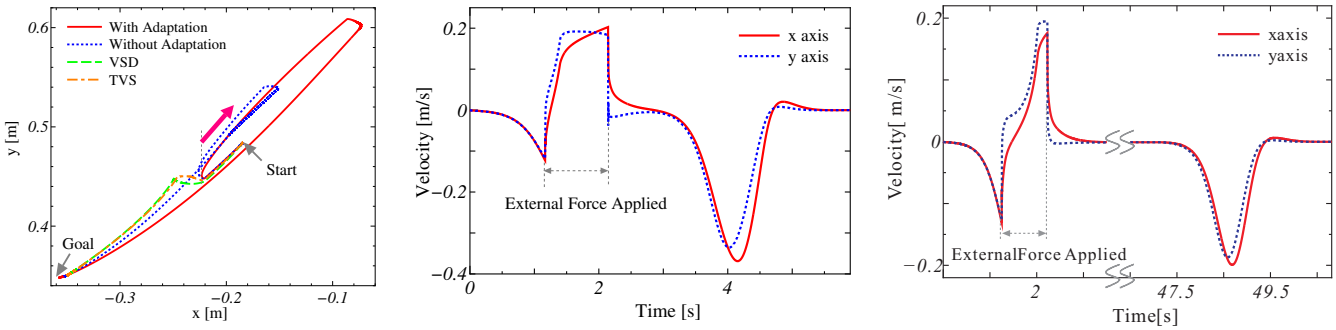

(*a*) Endpoint paths (*b*) Endpoint speed profile with adaptation (*c*) Endpoint speed profile without adaptation

Fig. 10. Simulation results: $\boldsymbol{F}_e = [1.0\ 1.0]^T$ (N) is applied temporally to the manipulator's endpoint

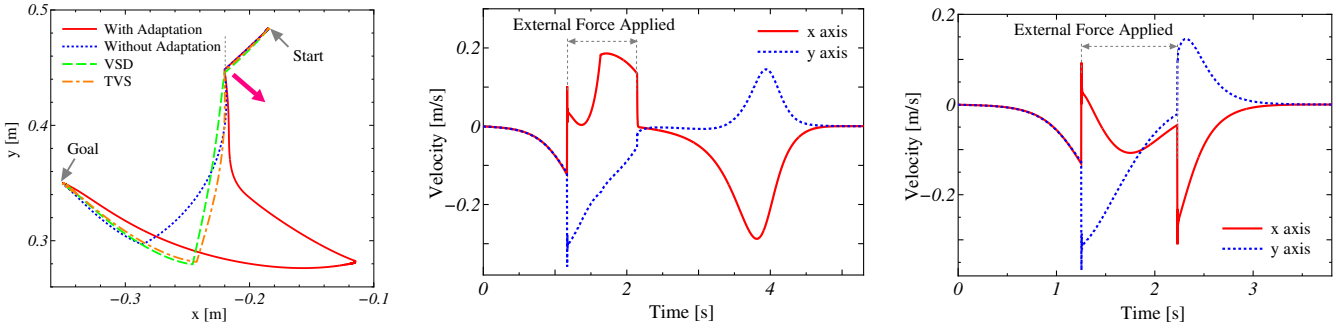

(*a*) Endpoint paths (*b*) Endpoint speed profile with adaptation (*c*) Endpoint speed profile without adaptation

Fig. 11. Simulation results: $\boldsymbol{F}_e = [1.0\ -1.0]^T$ (N) is applied temporally to the manipulator's endpoint

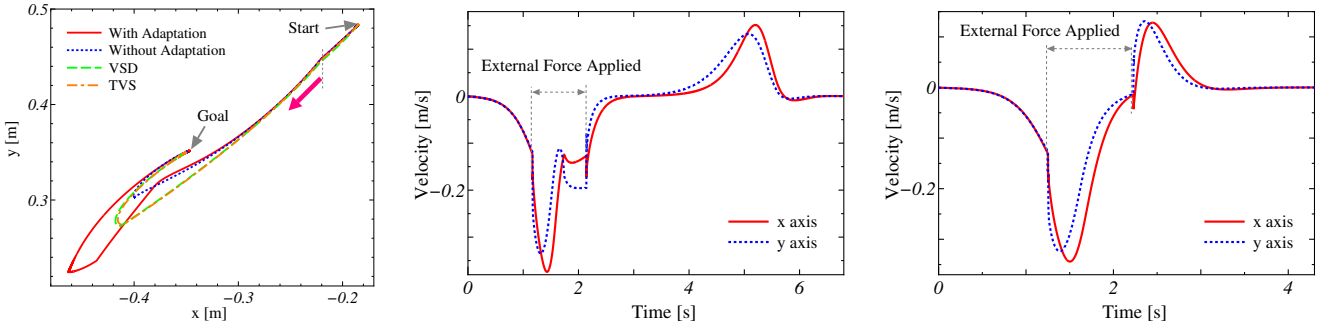

(*a*) Endpoint paths (*b*) Endpoint speed profile with adaptation (*c*) Endpoint speed profile without adaptation

Fig. 12. Simulation results: $\boldsymbol{F}_e = [-1.0\ -1.0]^T$ (N) is applied temporally to the manipulator's endpoint

V. Conclusion

The nonlinear reference shaping controller was proposed based on the virtual spring-damper hypothesis. The online parameter tuning approach was also proposed for generating smooth reaching movement.

In this paper, we proposed two adaptation methods; "slow adaptation" and "rapid adaptation", applied onto the apparent initial endpoint position, which is used to the online parameter tuning. These made smooth endpoint speed profiles and movements flexible to follow applied external force. It also accomplished smooth restart of reaching movement in the case that the significant change of the current endpoint position is generated by excessive external force. Furthermore, continuous reaching movements are obtained while the target endpoint position is changed during the movements.

Explicit inclusion of time is not needed for the proposed method, so that it can be implemented in the existence of external force/disturbance. It also realizes the movement flexible along the external force/disturbance without detecting them, just only using information of $\boldsymbol{x}$, $\boldsymbol{x}_g$ and $\boldsymbol{x}_o$. It is the advantage of the proposed method over VSD/TVS and other methods for controlling of the manipulator which shares its workspace with humans.

Acknowledgment

The authors thank Dr. Hideaki Yamato for his valuable comments and suggestions.

Appendix

Lagrange's equation of motion of the manipulator is described by

$$\boldsymbol{H}\ddot{\boldsymbol{\theta}} + \left\{\frac{1}{2}\dot{\boldsymbol{H}} + \boldsymbol{S}\right\}\dot{\boldsymbol{\theta}} = \boldsymbol{\tau}. \tag{8}$$

$\boldsymbol{H} \in \mathbb{R}^{m\times m}$ is the inertia matrix and $\boldsymbol{S} \in \mathbb{R}^{m\times m}$ the skew-symmetric matrix. Consider the following control signal:

$$\boldsymbol{\tau} = -\left(\frac{\partial U}{\partial \boldsymbol{\theta}}\right)^{\mathrm{T}} - \boldsymbol{D}\dot{\boldsymbol{\theta}}. \tag{9}$$

$\boldsymbol{D} = \boldsymbol{C} + \boldsymbol{J}\boldsymbol{\xi}\boldsymbol{J}^{\mathrm{T}}$, $d = \|\boldsymbol{x}_g - \boldsymbol{x}\|$ and $U(d)$ is the positive definite function which equals 0 if and only if $d = 0$ i.e. $\boldsymbol{x} = \boldsymbol{x}_g$. The closed-loop dynamics of Eq.(8) and Eq.(9) is

$$\boldsymbol{H}\ddot{\boldsymbol{\theta}} + \left\{\frac{1}{2}\dot{\boldsymbol{H}} + \boldsymbol{S}\right\}\dot{\boldsymbol{\theta}} + \boldsymbol{D}\dot{\boldsymbol{\theta}} + \left(\frac{\partial U}{\partial \boldsymbol{\theta}}\right)^{T} = 0. \tag{10}$$

Let us define $\boldsymbol{u}$ by the left side of Eq.(10) and regard that $\boldsymbol{u} = \boldsymbol{0}$ is input to the system. We get the following equation:

$$\dot{\boldsymbol{\theta}}^{\mathrm{T}}\boldsymbol{u} = \dot{E} + \dot{\boldsymbol{\theta}}^{\mathrm{T}}\boldsymbol{D}\dot{\boldsymbol{\theta}}, \tag{11}$$

where E is defined as

$$E \equiv \frac{1}{2}\dot{\boldsymbol{\theta}}^{\mathrm{T}}\boldsymbol{H}\dot{\boldsymbol{\theta}} + U. \tag{12}$$

Since $E \geq 0$ for any $\boldsymbol{\theta}$ and $\boldsymbol{D}$ is guaranteed to be positive definite if $\boldsymbol{C}$ is positive definite and $\boldsymbol{\xi}$ is positive semi-definite, we get

$$\int_0^t \dot{\boldsymbol{\theta}}^{\mathrm{T}}\boldsymbol{u}\,\mathrm{d}t = E(t) - E(0) + \int_0^t \dot{\boldsymbol{\theta}}^{\mathrm{T}}\boldsymbol{D}\dot{\boldsymbol{\theta}}\,\mathrm{d}t \tag{13}$$

$$\geq -E(0), \tag{14}$$

which means that the system having $\boldsymbol{u}$ as input and $\dot{\boldsymbol{\theta}}$ as output is passive, so that $(d, \dot{\boldsymbol{\theta}}) = (0, 0)$, the equilibrium point of E, is asymptotically stable. Moreover, $\boldsymbol{x}$ asymptotically converges to $\boldsymbol{x}_g$ for $t \to \infty$.

From Eq.(2) - Eq.(4), remark that the proposed controller in this paper is equivalent to Eq.(9) by designing $U(d)$ as

$$U_1(d) \equiv k_p\left\{\frac{1}{2}d^2 - (1-\epsilon)\frac{d^3}{3d_o}\right\}, \tag{15}$$

where $\boldsymbol{K}_p \equiv k_p\boldsymbol{I}$, $d_o = \|\boldsymbol{x}_g - \boldsymbol{x}_o\|$ and $0 \leq d \leq d_o$. $U_1(d)$, obviously, is positive definite which equals 0 if and only if $d = 0$. Thanks to the adaptations, $d \leq d_o$ is always satisfied although external force is applied to the manipulator.

References

[1] S. Arimoto and M. Sekimoto. Human-Like Movements of Robotic Arms with Redundant DOFs: Virtual Spring-Damper Hypothesis to Tackle the Bernstein Problem. *Proc. of IEEE International Conference on Robotics and Automation*, pp. 1860–1866, 2006.

[2] W. Abend et al. Humam Arms Trajectory Formation. *Brain*, Vol. 105, No. 2, pp. 331–348, 1982.

[3] C. G. Atkeson and J. M. Hollerbach. Kinematic Features of Unrestrained Vertical Arm Movements. *The Journal of Neuroscience*, Vol. 5, No. 9, pp. 2318–2330, 1985.

[4] T. Flash and N. Hogan. The Cooedination of Arm Movements: An Experimentally Confirmed Mathmatical Model. *The Journal of Neuroscience*, Vol. 5, No. 7, pp. 1688–1703, 1985.

[5] Y. Uno et al. Formation and Control of Optimal Trajectory in Human Multijoint Arm Movement: Minimum Torque-Change Model. *Biological Cybernetics*, Vol. 61, No. 2, pp. 89–101, 1989.

[6] M. Sekimoto and S. Arimoto. Experimental Study on Reaching Movements of Robot Arms with Redundant DOFs based upon Virtual Spring-Damper Hypothesis. *Proc. of IEEE/RSJ Int. Conf. on Intelligent Robots and Systems*, pp. 562–567, 2006.

[7] F. Seto and T. Sugihara. Online Reference Shaping with End-point Position Feedback for Large Acceleration Avoidance on Manipulator Control. In *Proc. of IEEE/RSJ Int. Conf. on Intelligent Robots and Systems*, pp. 5743–5748, 2009.

[8] F. Seto and T. Sugihara. Nonlinear Reference Shaping with Endpoint Position Feedback for Large Acceleration Avoidance in Reaching Movement. In *Journal of Robotics and Mechatronics*, Vol. 22, pp. 173–178, 2010.

[9] F. Seto and T. Sugihara. Online Nonlinear Reference Shaping with End-point Position Feedback for Human-Like Smooth Reaching Motion. In *Proc. of the 9th IEEE-RAS Int. Conf. on Humanoid Robots*, pp. 297–302, 2009.

[10] R. Kikuuwe and H. Fujimoto. Proxy-Based Sliding Mode Control for Accurate and Safe Position Control. pp. 25–30, 2006.

[11] R. Kikuuwe et al. A Guideline for Low-Force Robotic Guidance for Enhancing Human Performance of Positioning and Trajectory Tracking: It Should Be Stiff and Appropriately Slow. *IEEE Tran. on Systems, Man and Cybernetics Part-A*, Vol. 38, No. 4, pp. 945–957, 2008.

[12] T. Tsuji et al. Biomimetic Trajectory Generation Based on Human Movements with a Nonholonomic Constraint. *IEEE Trans. on Systems, Man, and Cybernetics Part-A*, Vol. 32, No. 6, pp. 773–779, 2002.

[13] T. Tsuji et al. Bio-Mimetic Trajectory Generation of Robots via Artificial Potential Field with Time Base Generator. *IEEE Trans. on Systems, Man, and Cybernetics Part-C*, Vol. 32, No. 4, pp. 426–439, 2002.

[14] B. Hoff and M. A. Arbib. A Model of the Effects of Speed, Accuracy, and Perturbation on Visually Guided Reaching. In *Control of Arm Movement in Space*, pp. 285–306. Springer-Verlag, 1992.